 doi:10.20944/preprints202107.0162.v1

Article

Influence of N_2 Flows on Sputtered Ta(N) films: Electrical, Structural, Chemical and Optical Properties

Yingying Hu [1], Md Rasadujjaman [1,2,*], Yanrong Wang [1], Jing Zhang [1], Jiang Yan [3,*] and Mikhail R. Baklanov [1,4]

[1] Department of Microelectronics, North China University of Technology, Beijing 100144, China; hyy_yingying@163.com (Y.Y.H.); wangyanrong@ncut.edu.cn (Y.W.); zhangj@ncut.edu.cn (J.Z.); m_baklanov@hotmail.com (M.R.B.)
[2] Department of Physics, Dhaka University of Engineering & Technology, Gazipur 1707, Bangladesh
[3] High-Tech Innovation Institute, North China University of Technology, Beijing 100144, China
[4] Research and Education Center "Technological Center", MIREA—Russian Technological University, 119454 Moscow, Russia
* Correspondence: rasadphy@duet.ac.bd (M.R.); yanjiang@ncut.edu.cn (J.Y.)

Abstract: By reactive DC magnetron sputtering from a pure Ta target onto silicon substrates, Ta(N) films were prepared with a different N_2 flow rate of 0, 12, 17, 25, 38, 58 sccm. The effects of N_2 flow rate on the electrical properties, crystal structure, elemental composition and optical properties of Ta(N) were studied. These properties were characterized by the four-probe method, X-ray diffraction (XRD), X-ray photoelectron spectroscopy (XPS), and spectroscopic ellipsometry (SE). Results show that the deposition rate decreases with an increase of the N_2 flows. On the other hand, the resistivity increases, the crystal size decreases, and the crystal structure transitions from β-Ta to TaN(111), and finally becomes the N-rich phase Ta_3N_5 (130,040). Studying the optical properties, it is found that there are differences in the refractive index (n) and extinction coefficient (k) of Ta(N) with different thicknesses and different N_2 flow rates, and dependent on the crystal size and crystal phase structure.

Keywords: tantalum nitride; electrical properties; structural properties; elemental composition; spectroscopic ellipsometry; optical properties

1. Introduction

Transition metal nitrides, especially tantalum nitride (TaN) are highly demanded in a wide range of applications due to their high melting point, hardness, excellent wear and corrosion resistance, refractory character, mechanical and high-temperature stability, chemical inertness, and histocompatibility [1–6]. Some prominent examples of such applications as a protective coating material for protection against oxidation and corrosion [7], as a diffusion barrier for Al and Cu metallization in advanced microelectronics [8–11], in phosphide and nitride optoelectronics as ohmic contact [3,4], in artificial heart valves as histocompatibility materials [12], thin film resistor [13], as ceramic pressure sensors [14], and also different mechanical applications [5,6]. The large interest for TaN arises since it is considered recently as a high thermal conductive material in microelectronic chips for the θ-TaN phase [15].

Furthermore, TaN belongs to the class of complex nitride phases of compounds which can vary from stoichiometry due to lattice vacancies. Diversifications in phase structure were common in TaN, from hexagonal-Ta_2N, cubic-TaN, hexagonal-TaN, hexagonal-Ta_5N_6, tetragonal-Ta_4N_5 and orthorhombic-Ta_3N_5 including TaN, which led to large differences in physical, chemical, and mechanical properties. The TaN alloy forms a variety of phases depending on the deposition technique and growth conditions [16,17].

 doi:10.20944/preprints202107.0162.v1

Numerous reports have been published to characterized sputtered TaN films based on various sputtering parameters such as nitrogen (N_2) partial pressure ratio [18,19], N_2/Ar flow rate ratio [20–22], sputtering power [23], and substrate temperature [24] during deposition. By controlling these different parameters, the influence on the structural, chemical, electrical, and optical properties of the TaN film have been investigated.

Among them, there are quite a few studies on how the N_2 flow or N_2/Ar flow rate ratio and the $N_2/(N_2+Ar)$ partial pressure ratio affect the properties of the TaN film. Chen et al. [25] used a magnetron sputtering low-power radio frequency deposition method with variable nitrogen flow rate to deposit TaN_x barrier layers on silicon. They found that as the N_2 flow rate increases, the surface roughness of the deposited TaN_x film was slightly increased, and the amorphous structure of TaN_x was formed with good thermal stability. Zaman et al. [26] prepared a TaN film with a 3% to 25% $N_2/(N_2+Ar)$ ratio on Si substrate by reactive magnetron sputtering and studied the effect of N_2 partial pressure on the crystal structure and hardness of the TaN film. It was found that the deposited films with 5% and 3% N_2 content showed the highest hardness (33 Pa).

Although sputtered TaN films have been widely investigated for their different properties, their optical properties have not been analyzed yet much. Recent studies have shown that spectroscopic ellipsometry (SE) can be used to characterize and measure the thin film thickness because of its fast and non-destructive nature [2,27–29]. Aouadi et al. [2] have studied the effects of varying N_2 flow rates from 1 to 4 sccm on the structural and optical properties of TaN thin films. They report that the optical constants (ε_1, ε_2) will be used in conjunction with real-time SE to monitor and control the growth of tantalum nitride films. Cherfi et al. [30] deposited TaN films with an N_2 flow rate of 0-12 sccm on Si (100) and glass substrates by DC magnetron sputtering, and shown that the influence of nitrogen flow on the crystal structure and optical properties of TaN. It was shown that for low N_2 flow (1 and 2 sccm), the TaN films show good conductor performance; a further increase of N_2 flow shows non-metallic behavior. At the same time, samples with similar structural properties have similar behaviors in terms of optical properties. Waechtler et al. have been shown that SE can be used to examine the optical properties of Ta and TaN thin films from 75 nm to 380 nm thickness. They have found a good agreement of optical properties with narrow-band data available for similar thin films. It was also shown that the optical properties of the films strongly depends with both substrate and film thickness [27]. Ma et al. have been studied the temperature-dependent dielectric function of TiN films by SE [28]. Recently, Xu et al. [31] used the method of comparing the measured refractive index of the low-k film under the Ta(N) diffusion barrier with the refractive index of the blank low-k film to study the integrity of the Ta(N) diffusion barrier using the approach developed by Shamiryan et al. [32].

However, there has been limited study of the optical behavior of the different stoichiometric of thicker TaN films by SE with varying N_2 flow rates in conjunction with electronic, structural and chemical composition. The study of the optical properties of TaN can provide us with more information about TaN films and some potential possibilities for the development of new applications. So, the systematic study of TaN films for understanding the electrical, structural, chemical composition and optical properties are required.

Therefore, we first focus our attention on the optical properties of TaN films by SE, a non-destructive testing method. By examining the optical properties of the sample, it can provide some guidance for the deposited sample. At the same time, from the existing research on the optical properties of TaN films, people ignore the influence of refractive index (n) and extinction coefficient (k), let alone explore the influence of process conditions on them, but they are also important optical parameters. Because the refractive index (n) and extinction coefficient (k) are regarded as "fingerprints of thin film materials." Then, the effects of deposition rate and N_2 flow on Ta(N) films deposition on the electrical, structure, elemental composition and optical properties (n & k) of TaN films were studied by using the four-probe method, X-ray diffraction (XRD), X-ray photoelectron spec-

 doi:10.20944/preprints202107.0162.v1

troscopy. The observation of different phases and chemical composition evaluation observed by XRD, XPS are correlated with optical properties.

2. Materials and Methods

Ta(N) films were synthesized using a standard magnetron sputtering (JS35-80G) system with sputtering non-uniformity is ≤ ±5%. The Ta(N) films were deposited on Si (100) wafers using magnetron sputtering of a Ta target (8.0 cm in diameter and 6.0 mm thick) of 99.95% purity. The substrate holder (located in the center of the chamber) was a 25 cm diameter plate, with rotation set to 10 rpm without heating the substrate for all of the depositions to improve the uniformity of the films. The target to substrate distance was 13.0 cm, and a negative bias was applied to the Ta target. After placing the Si(100) substrate in the deposition chamber, the chamber was evacuated to 9.6×10^{-4} Pa (by a turbo-molecular pump), the background vacuum was sufficient to ensure the vacuum required for Ta(N) film sputtering. Ar (99.999% purity) and N_2 (99.999% purity) were introduced into the reaction chamber through a mass flow controller and used as sputtering and reaction gases, respectively. The Ta target and the Si-substrate were sputter cleaned with Ar plasma prior to the Ta(N) films deposition for 5 min. Following cleaning, Ta(N) film was deposited at 9.56×10^{-4} Pa background pressure and 200 W DC applied power in a mixture of Ar and N_2.

To study the influence of different N_2 flow rates on the properties of the sputtered Ta(N) film, in all sputtering processes, the flow rate of Ar was fixed at 58 sccm with various N_2 flow rates from 0 to 58 sccm. The ratio of the reactive gas (N_2, 0–58 sccm) to the sputter gas (argon, 58 sccm) were varied from 0, 0.20, 0.29, 0.43, 0.65, 1.00. The deposition time was also varied from 10 to 30 min to study whether the thickness of the film affects the optical and other properties of Ta(N) under each N_2 flow rate. Among them, when the N_2 flow is 12 sccm and 17 sccm, we only sputtered for 10 min respectively.

The thickness of the film was measured by a German Bruker Dektak step meter. The thickness was determined from the step height between the film and a masked substrate area. The resistivity of the sample was measured by a double-electric four-point resistance resistivity tester (FT-341) and was obtained from the current between two external probes and measuring the voltage through the internal probes.

The crystallographic structure of the sputtered Ta(N) films was measured by an x-ray diffractometer (Rigaku Ultima IV, Japan) using a θ–2θ scan with a 1.54 Å wavelength Cu Kα radiation, at room temperature, working at 40 kV and 30 mA, and record the diffraction intensity in the scattering angle range of 20–60°.

X-ray photoelectron spectroscopy (XPS) was used to investigate the elemental composition and chemical states in Ta(N) films using PHI 5300 (PerkinElmer, USA) with an Mg Kα (1253.6 eV) excitation source. This source was operated using a voltage of 12.5 kV and an emission current of 20 mA. The films were sputter cleaned in an Ar^+ environment with 89.45 eV pass energy for 5 min prior to measurement. Survey scans were conducted in the 0–1100 eV range.

The optical characterization of the films was carried out using a SENpro spectroscopic ellipsometer (SENTECH, Germany) to measure ellipse deflection phase (Δ) and amplitude (Ψ) angles at an incident angle of 70° in the spectral range from 400 nm to 1050 nm at 5 nm increments. In all cases, the ellipsometric data were processed using SpectraRay/3 software for the data analysis. By treating the Ψ–Δ spectra, the refractive index (n) and extinction coefficient (k) of the corresponding Ta(N) films were extracted by using E. Kondoh ELLIPSHEET [33] for an infinitely thick film. The validity of this approach will be proved below in the ellipsometry part of this paper. The specific details and film thickness are given in Table 1.

Preprints (www.preprints.org) | NOT PEER-REVIEWED | Posted: 6 July 2021 doi:10.20944/preprints202107.0162.v1

Table 1. The thickness, sheet resistance and resistivity of Ta(N) film deposited with different N_2 flow rates and different sputtering times.

Film	Sputtering time (min)	Argon flow (sccm)	N_2 flow (sccm)	Thickness (nm)	Sheet resistance (Ω/sq)	Resistivity (μΩ.cm)
Ta	10	58	0	223.18	8.67	193.5
	20			449.63	4.39	197.4
	30			664.35	2.92	193.9
TaN	10	58	12	159.00	33.03	524.00
TaN	10	58	17	150.00	47.18	738.00
TaN	10	58	25	161.07	63.23	1018.4
	20			282.08	55.57	1567.5
	30			439.51	32.10	1410.8
TaN	10	58	38	129.84	2090.0	27136.6
	20			246.84	1020.0	25177.7
	30			399.00	174.83	6975.7
TaN	10	58	58	97.64	160.70	1568.9
	20			195.93	7480	146555.6
	30			305.19	13200	402850.8

3. Results and discussion

3.1. Deposition rate and resistivity

The deposition rate of Ta(N) films, sheet resistance and resistivity depend on the flow of nitrogen. The film thickness decreases with increasing the flow of nitrogen, as shown in Figure 1a and the increase of sputtering time from 10 min to 30 min makes the film thicker. However, the deposition rate does not depend on the sputtering time (Figure 1b). With the increase of nitrogen flow in the sputtering atmosphere of ionized Ar+, the intensity of ion bombardment of Ta target decreases due to the reduction of mean free path length and the number of sputtered Ta atoms also decreases leading to a gradual reduction in deposition rate [34]. In addition, since there are a large number of active N atoms in the sputtering atmosphere (an increase of the N_2 flow rate), the number of active N atoms in the atmosphere gradually increases, which increases the chemical reaction between active N atoms and the surface of the Ta target. The probability of TaN compound causes slight poisoning of the target [35,36], thereby reducing the sputtering rate.

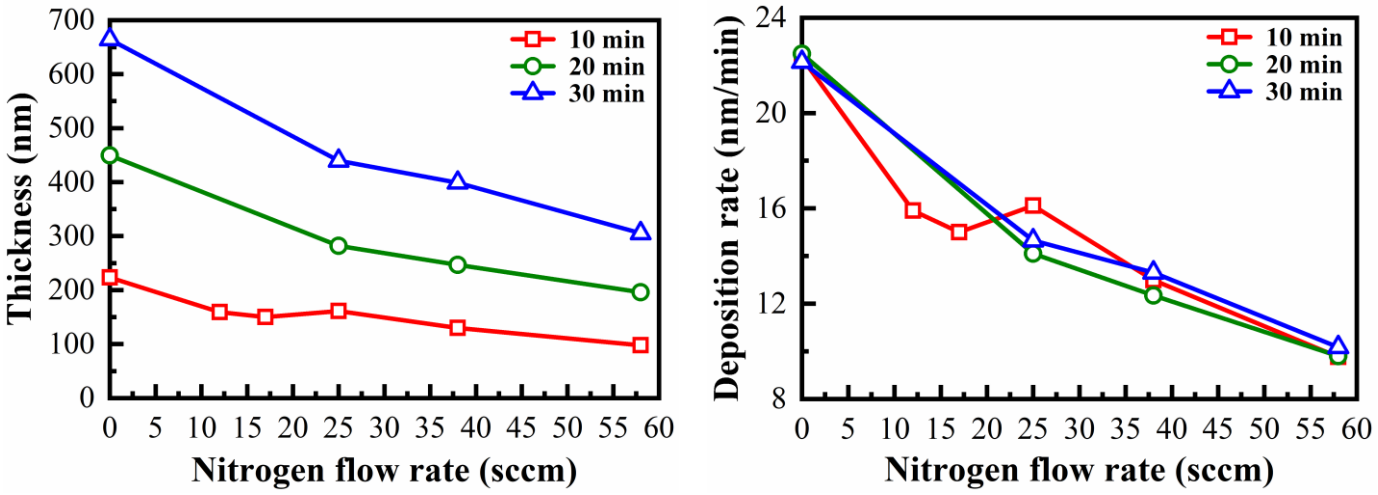

Preprints (www.preprints.org) | NOT PEER-REVIEWED | Posted: 6 July 2021 doi:10.20944/preprints202107.0162.v1

(a) (b)

Figure 1. Change of Ta(N) film thickness measured by Dektak step meter (a) and the deposition rates (b) for different nitrogen flows and sputtering time.

The electrical resistivity of pure Ta films sputtered for 10, 20 and 30 min are nearly same (193.5, 197.4, and 193.9 μΩ-cm, respectively (Table 1)). It is interesting to notice that the measured resistivity for pure Ta films are similar to the values reported for tetragonal crystalline Ta (β-Ta) films (165 μΩ-cm, Schauer et al. [37]; 210 μΩ-cm, Cuong et al. [38]) and 242 μΩ-cm, Arshi et al. [39]). Therefore, our pure Ta films are most likely β-Ta. The electrical resistivity of Ta(N) films deposited with different nitrogen flows is shown in Figure 2. It can be seen that the resistivity of TaN is higher than the resistivity of pure Ta observed at zero nitrogen flow. Introduction of nitrogen increases resistivity: first, it changes linearly (embedded graph) and thinner film has lower resistivity. The trend of increased resistivity can be attributed to the decreasing of the low resistivity Ta phase in the deposited Ta-N films and to the increasing of the low resistivity N-rich TaN phase. A much more dramatic change of resistivity is observed in the films deposited with 58 sccm N_2 flow, especially after 30 min deposition (relatively thick films, see Table 1).

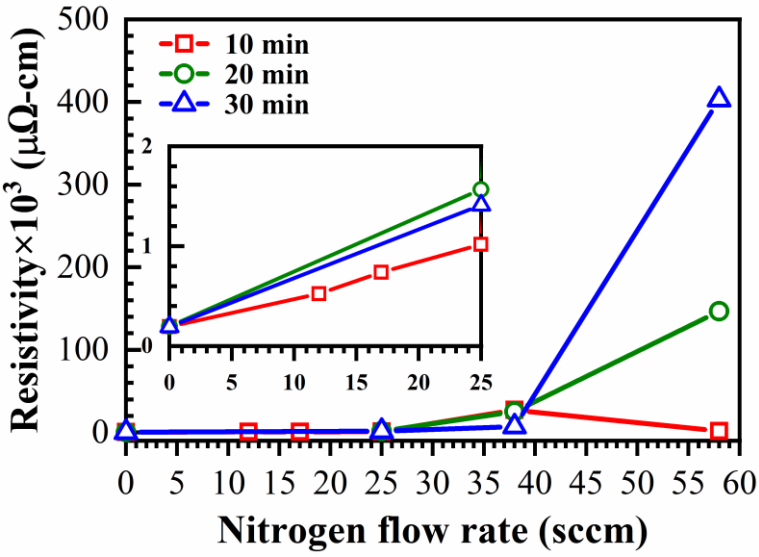

Figure 2. The resistivity TaN films at different nitrogen flow. The embedded graph is a zoom of data corresponding to low nitrogen flow region.

Further increase of N_2 flow increases the resistivity of Ta(N) film and might depend on the formation of different surface topography, grain size, changes of composition, amorphous structure formation and defects/imperfection (scattering from grain boundary) [40]. The resistivity of TaN films in the current work is similar to the values observed in the literature [40,41]. When the N_2 flow rate is 12 sccm, the resistivity of the sputtered TaN film is increased to 524 μΩ-cm and close to FCC TaN [42–45], or cubic TaN(111) [39] or Ta_3N_5 or Ta_5N_6 [46–48]. After a further increase in the nitrogen flow to 25 sccm, the resistivity of the sputtered TaN film is close to the resistivity of Ta_3N_5 (1126 μΩ-cm, [39]). Remarkably, when the increase of N_2 flow was increased to 38 and 58 sccm, the resistivity of the sputtered TaN films drastically increased, with only exception of 10 min deposition TaN films. Normally, it can be explained by increasing electron scattering from interstitial N atoms. [39]. However, this model does not explain so strong difference between the films deposited with 38 and 58 sccm [49]. It is also well-known that an excess of N_2 flow rate will decrease the mean free path of ionized Ta atoms and disturb the formation of TaN structures [40,50] and also increased electron scattering from interstitial N atoms. Therefore, the phase of the TaN film generated under our N_2 flow rate will also be dif-

Preprints (www.preprints.org) | NOT PEER-REVIEWED | Posted: 6 July 2021 doi:10.20944/preprints202107.0162.v1

ferent. The existence of N-rich phases in the TaN films at higher nitrogen flows is consistent with both the XRD patterns and the XPS analysis.

3.2. Structural Properties (XRD Analysis)

Figure 3 shows the X-ray diffraction (XRD) patterns of the Ta(N) films deposited for 10 min, 20 min, and 30 min with different N_2 flows in the gas mixture varying from 0 to 58 sccm. The XRD spectra of the Ta films (N_2 flow rate is 0) shows a mixed phase of β-Ta (221), β-Ta (002), β-Ta (330), and Ta(110), among which β-Ta The diffraction intensity of (002) is the highest, and the peak area of the diffraction peak is the largest, which indicates that the Ta film we sputtered is mainly β-Ta (002) preferred orientation (PDF#: 04-0788). Peaks at 35.40°, 37.04° and 41.20° are indexed to be the TaN (111), TaN (111) [39], and TaN (200) (PDF#: 49-1283) structure respectively (Figure 3a). The peaks at 31.86°, and 35.10°corresponds to Ta_3N_5 (123) and Ta_3N_5 (130) or (040) compounds respectively [51].

When the N_2 flow rate is 12 and 17 sccm, a mixed phase of TaN (111) and TaN (200) appear, and the diffraction peak of Ta_3N_5 (023) also appears when the N_2 flow rate is 17 sccm. However, the diffraction peak of TaN (111) is the highest, and the diffraction peak area is also the largest, which indicates that the preferred orientation of the TaN film under these two flow rates is TaN (111). Similarly, when the N_2 flow rate is 38 and 58 sccm, the TaN film has a preferred orientation of Ta_3N_5 (130,040). At the same time, when the N_2 flow rate increases, the diffraction peaks gradually widen, which indicates that the grain size is gradually decreasing that leads to high resistivity Table 1 and correspondingly it could be attributed to the mixture of fcc TaN and amorphous structure [46,52,53]. These phenomena observed by XRD are in line with our previous conjectures in the section on resistivity and similar to those reported in an earlier study [43,44].

When the nitrogen flow rate is increased, the phase of the film evolved gradually from TaN(111) to Ta_3N_5 (130) or Ta_3N_5 (040) (35.40° to 35.03°) [51]. On the other hand, the TaN (200) peaks are gradually decreasing. A broad peak corresponding to Ta_3N_5 appeared for the 58 sccm sample and significant broadening of the peaks could be due to the formation of a two-phase nanocomposite structure. This can be attributed to the high nitrogen fraction, which is known to inhibit the crystallization of nitrogen rich TaN_x sputtered films. At the same time, the XRD patterns of TaN films with a nitrogen flow rate of 25–58 sccm and a sputtering time of 10–30 min were compared (Figure 3b and 3c), and it was found that the XRD patterns of TaN films with the same nitrogen flow rate but different sputtering times/different thicknesses did not change much, which shows that the thickness of the film does not affect the formation of the crystal structure of the film. Generally, the films deposited with 58 sccm of nitrogen do not have pronounced patterns and this suggests that the films are losing their crystalline structure and becoming more amorphous (Table 2).

Table 2. Calculated crystallite sizes of Ta and TaN films.

Flow rate of N_2 (sccm)	Peaks	Peak position, 2θ (deg)	FWHM, θ (deg)	Average crystalline size (nm)
0	β-Ta(002)	33.72	0.266	31.22
12	TaN(111)	35.40	0.340	24.54
17	TaN(111)	35.28	0.394	21.15
25	Ta_3N_5(130, 040)	35.04	0.543	15.34
38	Ta_3N_5(130, 040)	35.12	0.890	9.37
58	Ta_3N_5(130, 040)	34.24	3.394	2.45

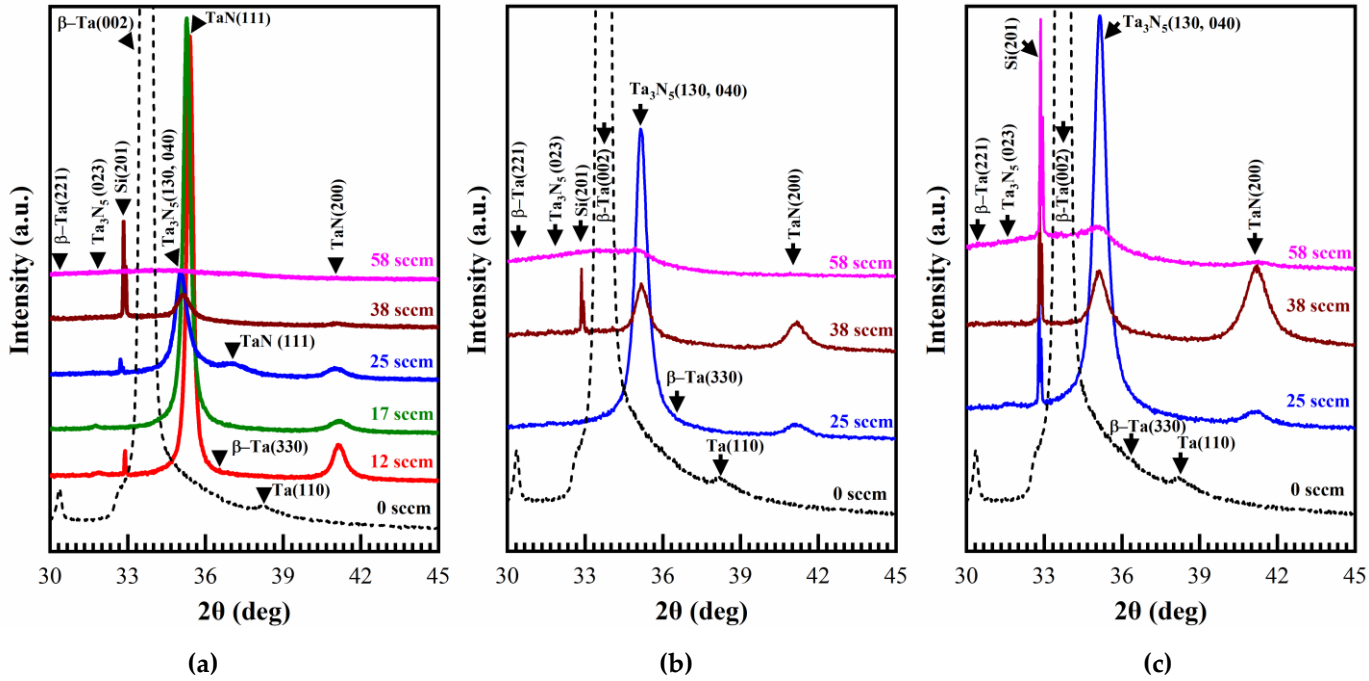

Figure 3. XRD patterns of Ta (20 min) and TaN films deposited for (**a**) 10 min, (**b**) 20 min, and (**c**) 30 min with different N_2 flows.

3.3. Elemental composition (XPS Studies)

XPS spectra was obtained to ascertain the elemental composition of the deposited TaN films. Figure 4 illustrates an evolution of the XPS survey spectrum of the deposited TaN films as a function of N_2 flow rate in the binding energy range of 0–1150 eV and show the Ta, O, N and C signals. It is confirmed that the survey does not contain additional component arises in the Si2p spectrum because our films were thicker. The unexpected O and C signal in these spectra might come from the ambient atmosphere in the sputtering chamber and/or the presence of background oxygen in the chamber during sputtering, and/or from organic residues during the storage, as already reported in literatures [35,39,54], also depends on different sputtering instruments, although there is a chemical shift for both O and C in the lower binding energy with increasing the N_2 flow rates due to the formation of Ta_2O_5 (Figure 5a and 5b).

Preprints (www.preprints.org) | NOT PEER-REVIEWED | Posted: 6 July 2021 doi:10.20944/preprints202107.0162.v1

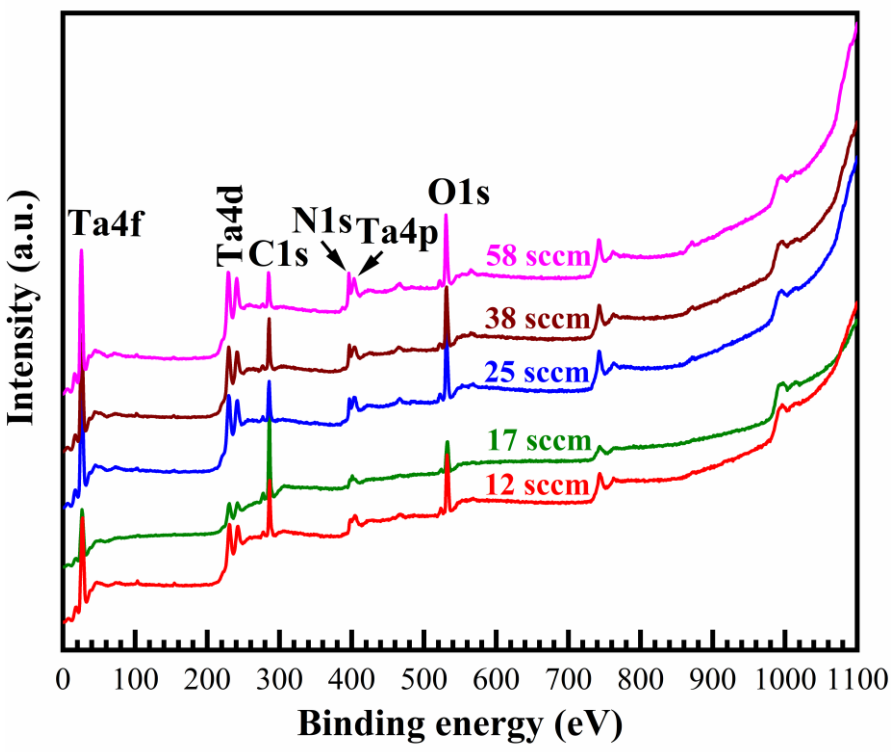

Figure 4. Evolution of the XPS survey spectra in the binding energy range of 0–1100 eV as a function of N_2 flows (12–58 sccm, 10 min deposition) showing the Ta, O, N and C signals for TaN films.

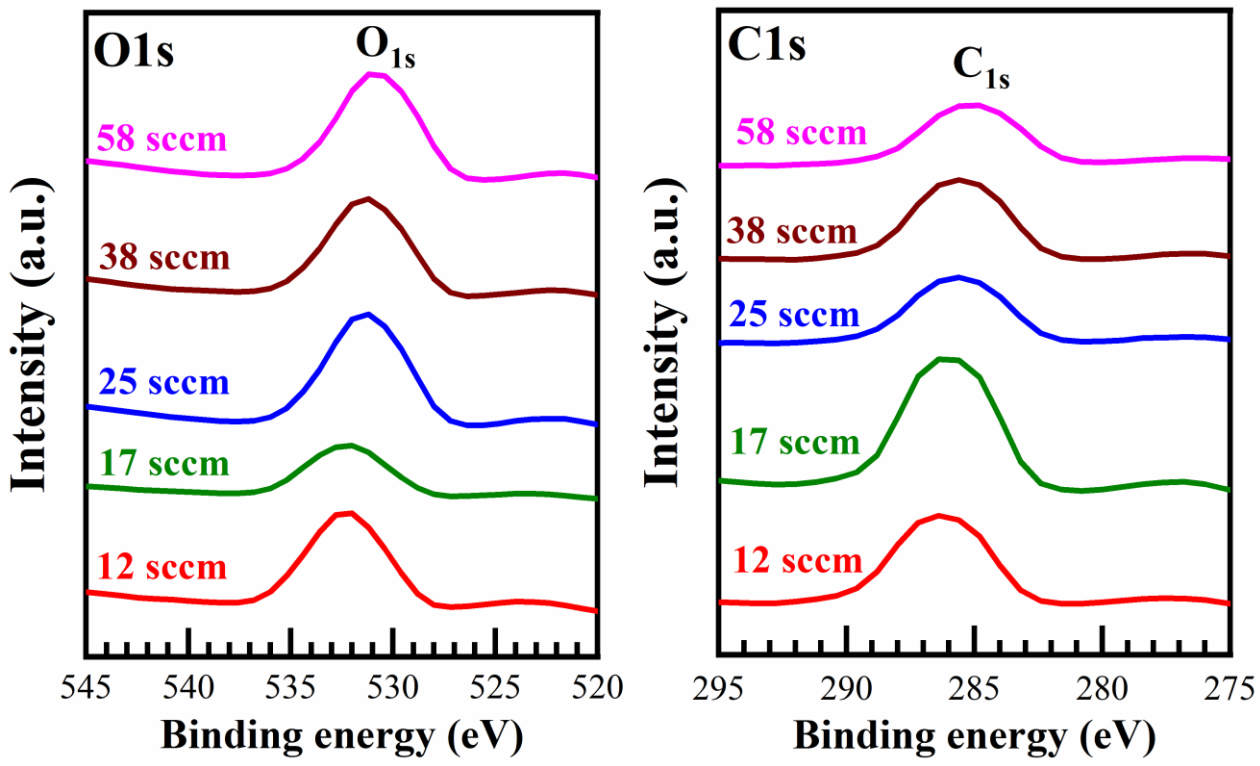

(**a**) (**b**)

Figure 5. XPS core levels spectra of (a) O1s, and (b) C1s for the TaN films at different N_2 flows (12–58 sccm, 10 min deposition).

 doi:10.20944/preprints202107.0162.v1

The XPS core-level spectra of Ta4f, Ta4d and N1s for different N_2 flow rates (12-58 sccm) were shown in Figure 6a, Figure 6b and Figure 6c, respectively. Figure 6a shows the XPS region of Ta4f, revealing that it is composed of three overlaying bonding environments: $Ta4f_{5/2}$ of Ta-O_x (Ta bonded with O), $Ta4f_{7/2, 5/2}$ of Ta-N and $Ta4f_{7/2}$ of Ta-N located at 30.25, 28.15, and 25.97 eV, respectively. As shown in Figure 6a, increasing the flow of N_2 from 12 to 58 sccm is likely to chemical shift the $Ta4f_{7/2}$ peaks from 25.97 to 25.78 eV, which were attributed to TaN $Ta4f_{5/2}$ peaks. On the other hand, the chemical shift from 30.25 to 29.81 revealing that O-rich films composed of Ta_2O_5 with an increase of N_2 flows were observed. Figure 7 shows the deconvoluted spectra of Ta4f for the TaN films with N_2 flow of 12 sccm. Compared with the Ta binding energy values of TaN and TaO_x in references, the binding energy values in the Ta4f spectrum ($Ta4f_{7/2}$ = 25.7 eV and $Ta4f_{5/2}$ = 27.7 eV) accorded with the chemical state of Ta in Ta–O binding [55]. The Ta4f doublet at binding energy $Ta4f_{7/2}$ = 27.3 eV and $Ta4f_{5/2}$ = 29.0 eV matched Ta^{5+} state in Ta_2O_5 [56,57], while the corresponding Ta4f doublet peaks are located respectively at $Ta4f_{7/2}$ = ~25.1 eV and $Ta4f_{5/2}$ = ~27.3 eV that should be attributed to N-rich TaN phase [58,59].

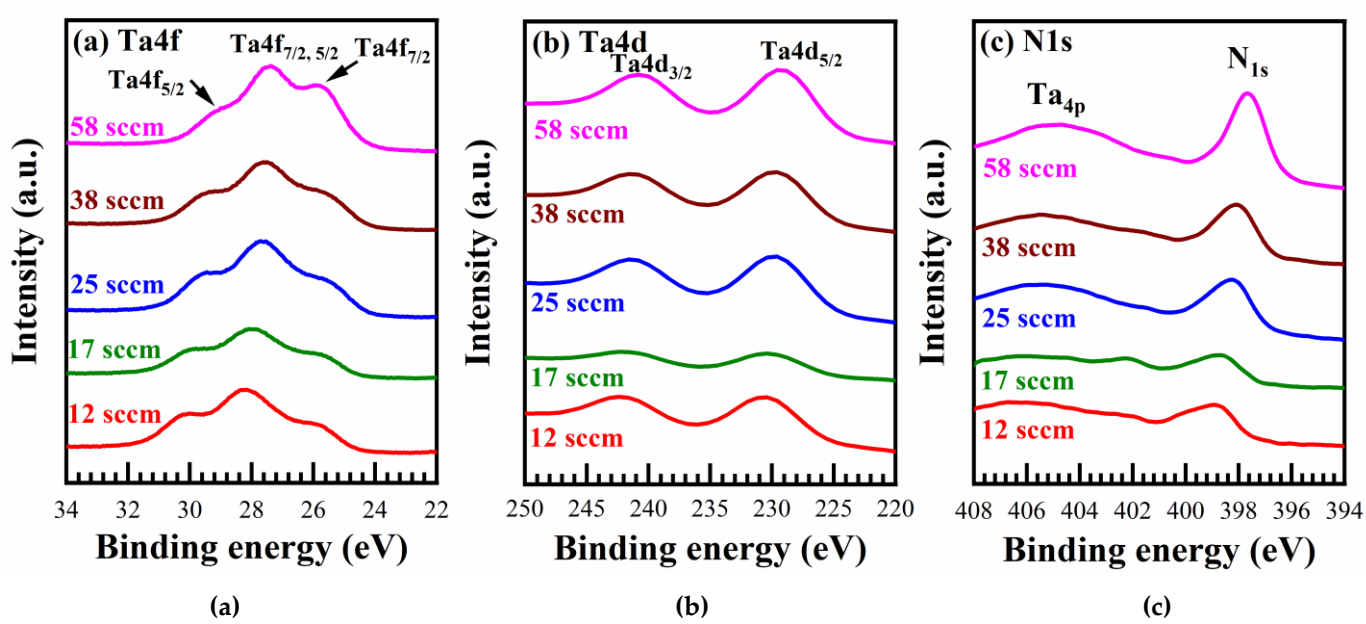

Figure 6. XPS core levels spectra of (a) Ta4f, (b) Ta4d and (c) N1s for the TaN films at different N_2 flows (12–58 sccm, 10 min deposition).

Preprints (www.preprints.org) | NOT PEER-REVIEWED | Posted: 6 July 2021 doi:10.20944/preprints202107.0162.v1

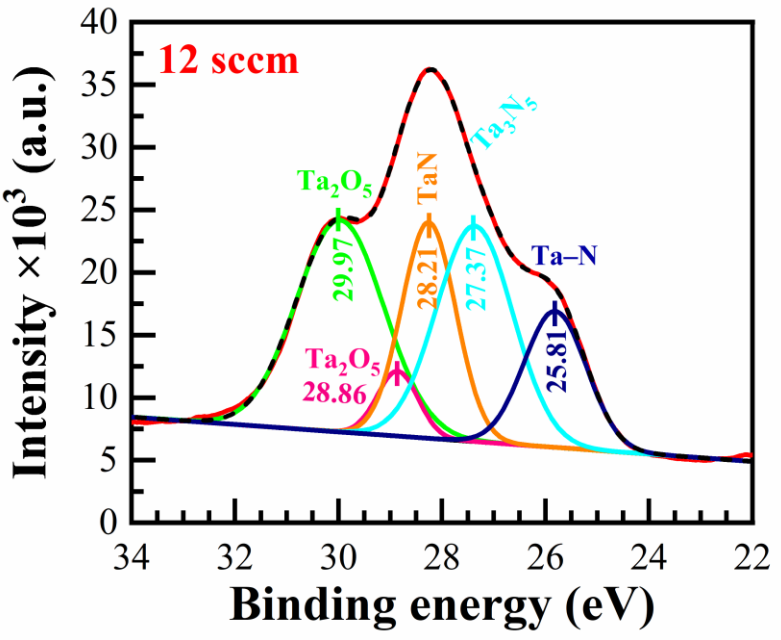

Figure 7. Deconvoluted spectra of Ta4f for the TaN films with N_2 flow of 12 sccm for 10 min deposition.

The existence of the Ta–N bonding in the film is further confirmed by the N1s peak located around 397.0 eV [60]. As the nitrogen flow rate increases, more Ta–N bonds form and the N1s peak also increases. This is consistent with the XRD spectra. It can be seen from Figure 6c that the N1s peak shifts from 397.55 to 398.85 eV for nitrogen flow from 12 to 58 sccm, while the $Ta4p_{3/2}$ peak also shifts from 406.4 to 404.95 eV. It is noteworthy that there are uncertainties on the exact value for Ta4p binding energy. Nyholm et al. reported a Ta4p value of 400.9 eV [61] and Tian et al. [62] reported a relatively high value of 406.0 eV. This shift in the binding energy for the N1s peaks toward lower values are in agreement with a previous study [35,39], while the binding energies for the Ta4f doublets also shift toward lower energy values and do not agree with previous studies.

3.3. Optical Properties

Spectroscopy ellipsometry (SE) is broadly used as an important tool for thin films thickness, refractive indices and optical properties analysis, and its basic principle is shown elsewhere [28]. For optically thick films, SE spectra can be fitted using a single layer (substrate model) and optical properties of the films can further be analyzed. As the refractive index (n) and extinction coefficient (k) cannot be measured directly and so must be calculated by some quantities that are related to them and can be directly measured. In this study, ellipsometry parameters Ψ and Δ were obtained by SE with Spectrumfit Levenberg-Marquardt + thickness scan fitting. Therefore, we measured the Ψ and Δ of all Ta films and TaN films by using only the substrate model, and extracted the n and k of the corresponding film by using E. Kondoh ELLIPSHEET [33].

Figures 8a and 8b depict the complex refractive index (n) and extinction coefficient (k), respectively for Ta films and with a comparison of the literature report. After comparing with the data of Tompkins et al. [63]. and Waechtler et al. [27], it is found that the changing trends of n and k of Ta films with different thicknesses are roughly the same, and the thickness does have an effect on the optical properties of Ta films. It is different from the conclusion that Waechtler et al. reported the same n, k of Ta films with different thicknesses.

Preprints (www.preprints.org) | NOT PEER-REVIEWED | Posted: 6 July 2021 doi:10.20944/preprints202107.0162.v1

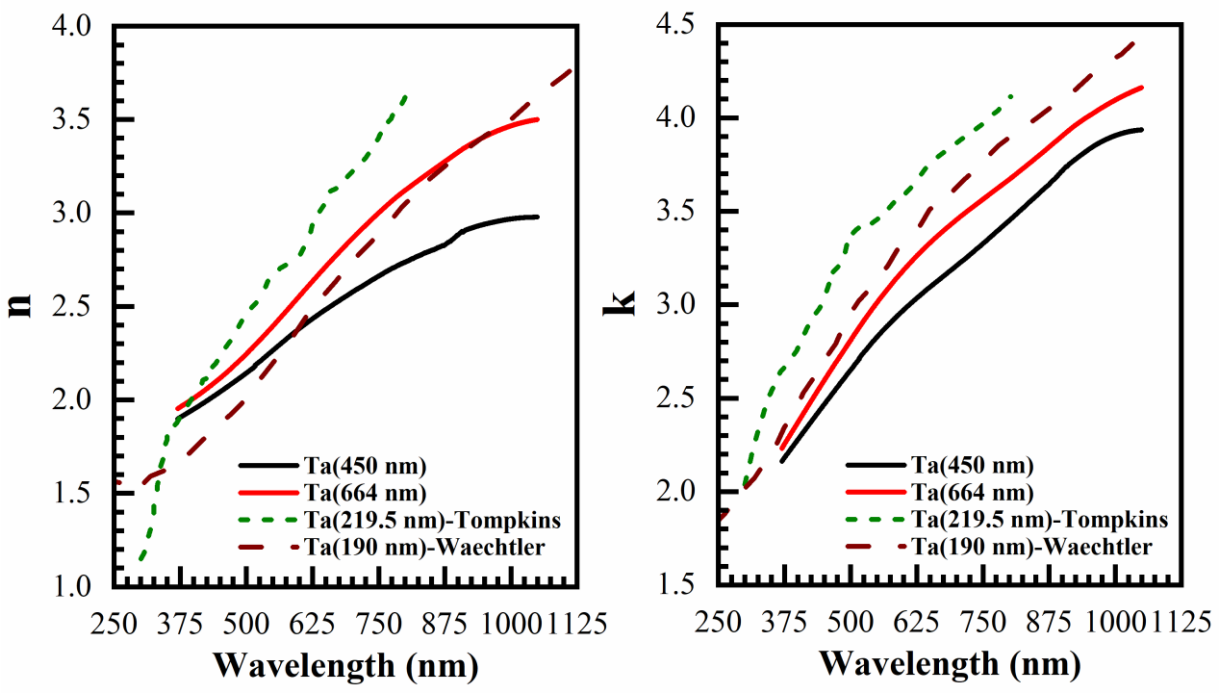

(a) (b)

Figure 8. Refractive index (n) and extinction coefficient (k) of Ta films sputtered for 20 min (450 nm) and 30 min (664 nm) are compared with literature data.

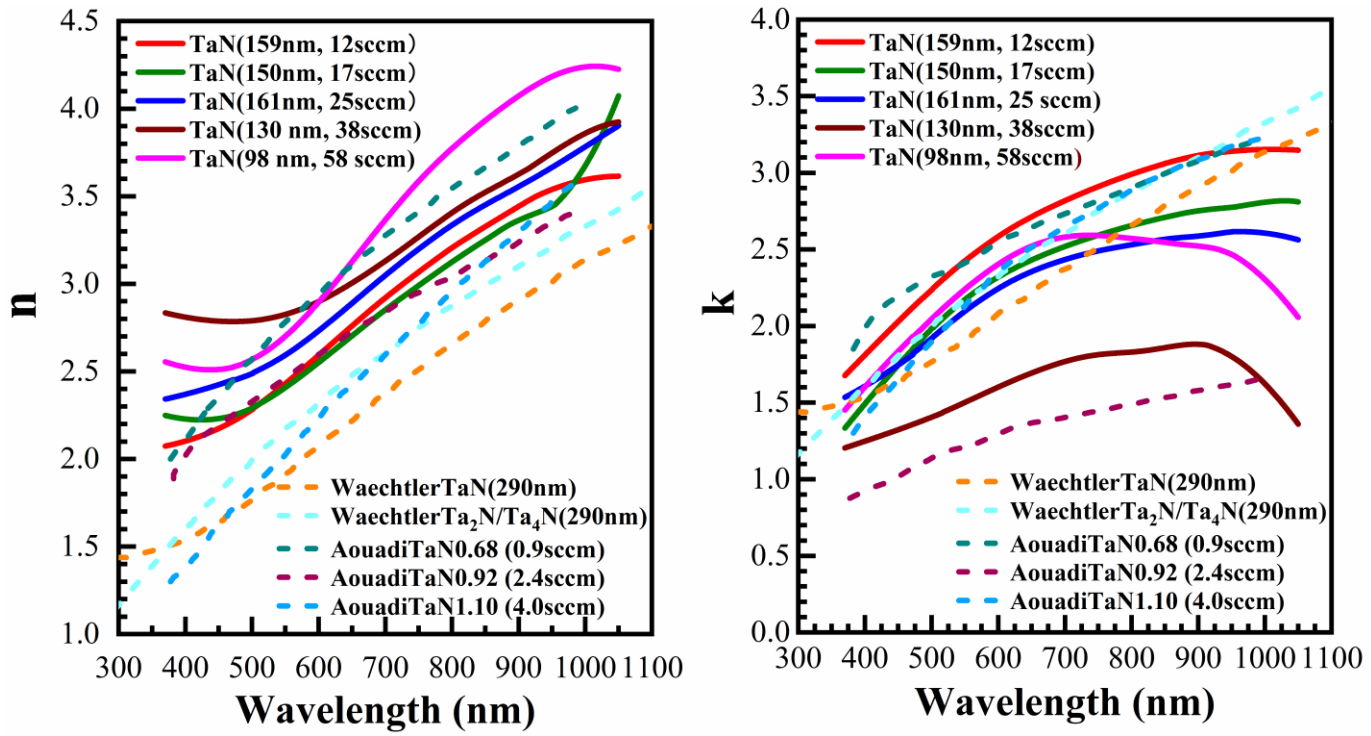

(a) (b)

Figure 9. The refractive index (n) and extinction coefficient (k) of TaN(12-58 sccm) films sputtered for 10 min are compared with those in the literature.

In Figure 9, we compare the refractive index (n) and extinction coefficient (k) of our sputtered TaN film with an N_2 flow rate of 12-58 sccm with the data of Aouadi et

Preprints (www.preprints.org) | NOT PEER-REVIEWED | Posted: 6 July 2021 doi:10.20944/preprints202107.0162.v1

al. [2] and Waechtler et al. [27]. Also, it is found that when the N_2 flow rate is 12 and 17 sccm, the n and k of our sputtered TaN film are close to the values in the reference, but as the N_2 flow rate increases, the n and k values of our sputtered TaN film are getting less and less close to the n and k values in the references (Fig. 9a and b). Besides, different N_2 flow rates and different thicknesses of TaN films have significant differences in n and k, which shows that both N_2 flow rate and thickness affect the optical properties of TaN. In addition, we can see that there are differences in the n and k values and curve shapes of TaN films with different crystal structures. The influence of N_2 flow rate on the n and k of TaN film may be caused by the different crystal structures and grain sizes of TaN film deposited with different N_2 flow rates. It is interesting that the extinction coefficient of TaN films deposited at high nitrogen flows (38 and 58 sccm) decreases starting from 700 nm and especially from 900 nm. The reduction of extinction coefficient suggests that the films are becoming more like dielectric and explains the drastic increase of their resistivity (Figure 2).

In this work, we used optically thick films to be able to extract optical characteristics. The thickness of these films are measured by using a Bruker Dektak step meter that also is used only for relatively thick film. However, many applications of Ta and TaN layers need very low thickness. For instance, when they are used as diffusion barriers in advanced microelectronics. Taking it into account we examined the applicability of ellipsometry to measure the thickness of the thin Ta and TaN layers. For this purpose, we used values of optical characteristics of these layers found in literature and measured in our work. Then we calculated Δ–Ψ trajectories for the films with the deferent thickness (Figure 10). The presented curves demonstrate that Ta(N) films thickness can be measured by ellipsometry when d ≤ 100 nm. The sensitivity is reduced with thickness but it can be very good for evaluation of Ta(N) films deposited as diffusion barriers for microelectronics application (d < 10 nm). It is also obvious that ellipsometry will be efficient for evaluation of the d < 100 nm films continuity as it was done in the Ref. [31,32].

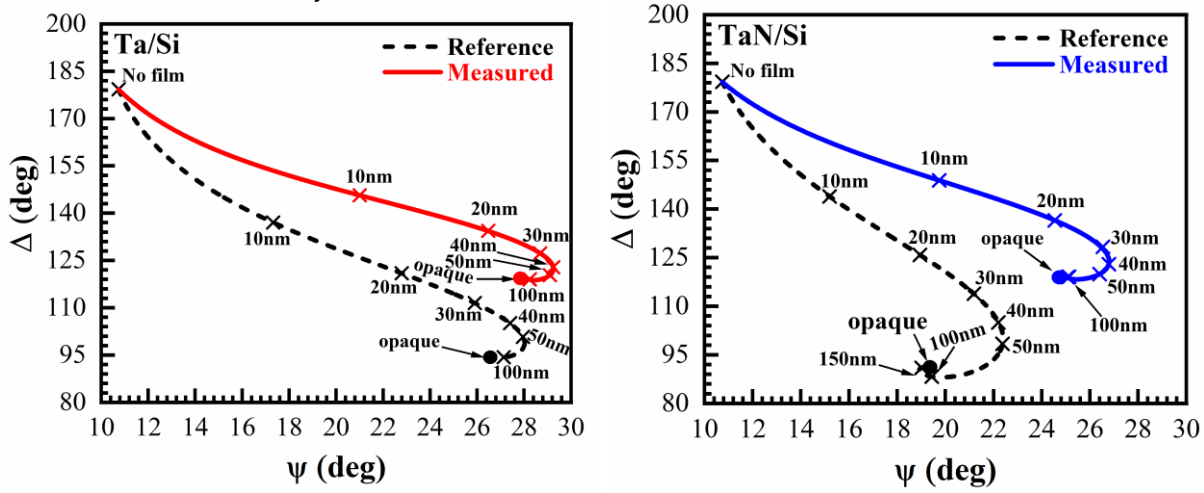

(a) (b)

Figure 10. Optical characteristics (the calculated Δ–Ψ trajectories) of deposited (a) Ta and (b) TaN films with different thicknesses. The solid curves were calculated by using optical characteristics at 633 nm measured in our films deposited with 12 sccm N_2. The dashed curves are based on optical characteristics reported in Ref. [27] (633 nm, Ar to N_2 ratio = 4:1, the flow rate is not reported).

4. Conclusions

The Ta(N) film with different N_2 flow rate (0-58sccm) and sputtering time of 10-30 min was deposited by the DC reactive magnetron sputtering method, and it was found that the deposition rate Ta(N) film, electrical, structural, chemical and

optical properties depend on N_2 flow rate. As the N_2 flow rate increases from 0 to 58 sccm, the crystal structure of the sputtered film transitions from β-Ta to TaN(111) and finally becomes the N-rich phase Ta_3N_5 (130) or Ta_3N_5 (040). When the N_2 flow rate increases, the diffraction peaks gradually widen, which indicates that the grain size is decreasing that's leads to higher resistivity (Table 1) and correspondingly it could be attributed to the mixture of fcc TaN and amorphous structure The films deposited with 58 sccm of nitrogen lose specific crystallographic patterns and therefore becoming amorphous. In the part of the optical properties study, we can see that both the thickness and the N_2 flow rate will affect the refractive index (n) and extinction coefficient (k) of TaN film, and have a greater impact on k. The curve shapes of n and k of similar crystal structures have a small difference. The influence of N_2 flow rate on the refractive index and extinction coefficient of TaN film may be caused by the different crystal structures and grain size of TaN film deposited with different N_2 flow rates. The extinction coefficient of the films deposited with 58 sccm of nitrogen decreases that suggests the formation of a more dielectric like nature of the deposited films. This fact explains the drastic increase the resistivity of the films shown in Figure 2. The reason for the transformation to the dielectric state is the incorporation of Ta oxide that can be seen from XPS data. When the nitrogen flow is so large, it reduces the free path length of sputtered atoms, poisons the Ta target and therefore reduces the effective deposition rate. As a result, the role of the residual oxygen is drastically increased and the deposited film is becoming Tantalum oxynitride with much higher resistivity. This effect is becoming more pronounced when the deposition time is long and this is the reason of the strong difference in resistivity between the films deposited during 10 min and 30 min. If deposition time is short, the target poisoning might be negligible.

Finally, the presented results suggest the resistivity of TaN films deposited by magnetron sputtering can be precisely controlled by changing nitrogen concentration during deposition. It is also important that a too high concentration of nitrogen might have a negative effect increasing the impact of gas phase impurities.

Author Contributions: Conceptualization, M.R.B.; methodology, Y.Y.H. and M.R.; software, Y.Y.H. and M.R.; validation, J.Z., J.Y. and M.R.B.; formal analysis, Y.Y.H., M.R., Y.W., J.Z., J.Y. and M.R.B.; resources, Y.W., J.Z., and J.Y.; data curation, Y.Y.H. and M.R.; writing—original draft preparation, Y.Y.H. and M.R.; writing—review and editing, Y.Y.H., M.R. and M.R.B.; visualization, Y.Y.H. and M.R.; supervision, Y.W., J.Z., J.Y. and M.R.B; funding acquisition, J.Z. and M.R.B. All authors have read and agreed to the published version of the manuscript.

Funding: This research was funded by the National Natural Science Foundation of China (NSFC), grant number 61874002 and Russian Foundation for Basic Research (RFBR), grant number 18-29-27022. The APC was funded by NSFC, grant number 61874002.

Institutional Review Board Statement: Not applicable.

Informed Consent Statement: Not applicable.

Data Availability Statement: Not applicable.

Acknowledgments: We would like to express sincere thanks to Professor Eiichi Kondoh from University of Yamanashi, Japan for his help to calculate the n and k from Δ and Ψ.

Conflicts of Interest: The authors declare no conflict of interest.

References

1. Han, J.H.; Kim, H.Y.; Lee, S.C.; Kim, D.H.; Park, B.K.; Park, J.-S.; Jeon, D.J.; Chung, T.-M.; Kim, C.G. Growth of tantalum nitride film as a Cu diffusion barrier by plasma-enhanced atomic layer deposition from bis((2-(dimethylamino)ethyl)(methyl)amido)methyl(tert-butylimido)tantalum complex. *Appl. Surf. Sci.* **2016**, *362*, 176–181, doi:10.1016/j.apsusc.2015.11.095.

2. Aouadi, S.M.; Debessai, M. Optical properties of tantalum nitride films fabricated using reactive unbalanced magnetron sputtering. *J. Vac. Sci. Technol. A Vacuum, Surfaces, Film.* **2004**, *22*, 1975–1979, doi:10.1116/1.1778410.
3. Kang, S.M.; Yoon, S.G.; Suh, S.J.; Yoon, D.H. Control of electrical resistivity of TaN thin films by reactive sputtering for embedded passive resistors. *Thin Solid Films* **2008**, *516*, 3568–3571, doi:10.1016/j.tsf.2007.08.027.
4. Lovejoy, M.L.; Patrizi, G.A.; Roger, D.J.; Barbour, J.C. Thin-film tantalum-nitride resistor technology for phosphide-based optoelectronics. *Thin Solid Films* **1996**, *290–291*, 513–517, doi:10.1016/S0040-6090(06)08966-8.
5. Shin, C.-S.; Kim, Y.-W.; Hellgren, N.; Gall, D.; Petrov, I.; Greene, J.E. Epitaxial growth of metastable δ-TaN layers on MgO(001) using low-energy, high-flux ion irradiation during ultrahigh vacuum reactive magnetron sputtering. *J. Vac. Sci. Technol. A Vacuum, Surfaces, Film.* **2002**, *20*, 2007, doi:10.1116/1.1513639.
6. Shin, C.-S.; Gall, D.; Kim, Y.-W.; Hellgren, N.; Petrov, I.; Greene, J.E. Development of preferred orientation in polycrystalline NaCl-structure δ-TaN layers grown by reactive magnetron sputtering: Role of low-energy ion surface interactions. *J. Appl. Phys.* **2002**, *92*, 5084–5093, doi:10.1063/1.1510558.
7. Patel, A.; Gladczuk, L.; Paur, C.S.; Sosnowski, M. Tantalum Nitride Seed Layers for Bcc Tantalum Coatings Deposited on Steel by Magnetron Sputtering. *MRS Proc.* **2002**, *750*, Y5.23, doi:10.1557/PROC-750-Y5.23.
8. Dalili, N.; Liu, Q.; Ivey, D.G. Thermal and electrical stability of TaN x diffusion barriers for Cu metallization. *J. Mater. Sci.* **2013**, *48*, 489–501, doi:10.1007/s10853-012-6763-x.
9. Volpi, F.; Cadix, L.; Berthomé, G.; Coindeau, S.; Encinas, T.; Jourdan, N.; Blanquet, E. Impact of silica-substrate chemistry on tantalum nitride thin films deposited by atomic layer deposition: Microstructure, chemistry and electrical behaviors. *Thin Solid Films* **2019**, *669*, 392–398, doi:10.1016/j.tsf.2018.10.006.
10. Liu, C.H.; Liu, W.; Wang, Y.H.; Wang, Y.; An, Z.; Song, Z.X.; Xu, K.W. Interface stability and microstructure of an ultrathin α-Ta/graded Ta(N)/TaN multilayer diffusion barrier. *Microelectron. Eng.* **2012**, *98*, 80–84, doi:10.1016/j.mee.2012.05.054.
11. Witt, C.; Yeap, K.B.; Lesniewska, A.; Wan, D.; Jordan, N.; Ciofi, I.; Wu, C.; Tokei, Z. Testing The Limits of TaN Barrier Scaling. In Proceedings of the 2018 IEEE International Interconnect Technology Conference (IITC); IEEE, 2018; pp. 54–56.
12. Leng, Y..; Sun, H.; Yang, P.; Chen, J..; Wang, J.; Wan, G..; Huang, N.; Tian, X..; Wang, L..; Chu, P.. Biomedical properties of tantalum nitride films synthesized by reactive magnetron sputtering. *Thin Solid Films* **2001**, *398–399*, 471–475, doi:10.1016/S0040-6090(01)01448-1.
13. Shostachenko, S.A.; Zakharchenko, R. V; Ryzhuk, R. V; Leshchev, S. V Thermal stability of tantalum nitride based thin film resistors. *IOP Conf. Ser. Mater. Sci. Eng.* **2019**, *498*, 012014, doi:10.1088/1757-899X/498/1/012014.
14. Ayerdi, I.; Castaño, E.; García-Alonso, A.; Gracia, J. High-temperature ceramic pressure sensor. *Sensors Actuators A Phys.* **1997**, *60*, 72–75, doi:10.1016/S0924-4247(96)01438-0.
15. Kundu, A.; Yang, X.; Ma, J.; Feng, T.; Carrete, J.; Ruan, X.; Madsen, G.K.H.; Li, W. Ultrahigh Thermal Conductivity of θ-Phase Tantalum Nitride. *Phys. Rev. Lett.* **2021**, *126*, 115901, doi:10.1103/PhysRevLett.126.115901.
16. Aouadi, S.M. Structural and mechanical properties of TaZrN films: Experimental and ab initio studies. *J. Appl. Phys.* **2006**, *99*, 053507, doi:10.1063/1.2178394.
17. Aouadi, S.M.; Bohnhoff, A.; Amriou, T.; Williams, M.; Hilfiker, J.N.; Singh, N.; Woollam, J.A. Vacuum ultra-violet spectroscopic ellipsometry study of single- and multi-phase nitride protective films. *J. Phys. Condens. Matter* **2006**, *18*, S1691–S1701, doi:10.1088/0953-8984/18/32/S01.
18. Nazon, J.; Sarradin, J.; Flaud, V.; Tedenac, J.C.; Fréty, N. Effects of processing parameters on the properties of tantalum nitride thin films deposited by reactive sputtering. *J. Alloys Compd.* **2008**, *464*, 526–531, doi:10.1016/j.jallcom.2007.10.027.
19. Tsukimoto, S.; Moriyama, M.; Murakami, M. Microstructure of amorphous tantalum nitride thin films. *Thin Solid Films* **2004**, *460*, 222–226, doi:10.1016/j.tsf.2004.01.073.

20. Bernoulli, D.; Müller, U.; Schwarzenberger, M.; Hauert, R.; Spolenak, R. Magnetron sputter deposited tantalum and tantalum nitride thin films: An analysis of phase, hardness and composition. *Thin Solid Films* **2013**, *548*, 157–161, doi:10.1016/j.tsf.2013.09.055.
21. Lee, W.-H.; Lin, J.-C.; Lee, C. Characterization of tantalum nitride films deposited by reactive sputtering of Ta in N2/Ar gas mixtures. *Mater. Chem. Phys.* **2001**, *68*, 266–271, doi:10.1016/S0254-0584(00)00370-9.
22. Wang, J.H.; Chen, L.J.; Lu, Z.C.; Hsiung, C.S.; Hsieh, W.Y.; Yew, T.R. Ta and Ta–N diffusion barriers sputtered with various N[sub 2]/Ar ratios for Cu metallization. *J. Vac. Sci. Technol. B Microelectron. Nanom. Struct.* **2002**, *20*, 1522, doi:10.1116/1.1495906.
23. Lee, T.; Watson, K.; Fen Chen; Gill, J.; Harmon, D.; Sullivan, T.; Baozhen Li Characterization and reliability of TaN thin film resistors. In Proceedings of the 2004 IEEE International Reliability Physics Symposium. Proceedings; IEEE; pp. 502–508.
24. Hantehzadeh, M.R.; Mortazavi, S.H.; Faryadras, S.; Ghoranneviss, M. The effect of temperature on the structure of tantalum nitride (TaN) thin films deposited by DC plasma. *J. Fusion Energy* **2012**, *31*, 84–88, doi:10.1007/s10894-011-9431-2.
25. Chen, S.-F.; Wang, S.-J.; Yang, T.-H.; Yang, Z.-D.; Bor, H.-Y.; Wei, C.-N. Effect of nitrogen flow rate on TaN diffusion barrier layer deposited between a Cu layer and a Si-based substrate. *Ceram. Int.* **2017**, *43*, 12505–12510, doi:10.1016/j.ceramint.2017.06.122.
26. Zaman, A.; Meletis, E. Microstructure and Mechanical Properties of TaN Thin Films Prepared by Reactive Magnetron Sputtering. *Coatings* **2017**, *7*, 209, doi:10.3390/coatings7120209.
27. Waechtler, T.; Gruska, B.; Zimmermann, S.; Schulz, S.; Gessner, T. Characterization of Sputtered Ta and TaN Films by Spectroscopic Ellipsometry. In Proceedings of the 2006 8th International Conference on Solid-State and Integrated Circuit Technology Proceedings; IEEE, 2006; pp. 2184–2186.
28. Ma, Q.; Shi, X.; Bi, L.; Li, J.; Zhou, Q.; Zhu, B. Influence of the deposition temperature on the optical and electrical properties of TiN film by spectroscopic ellipsometry. *Superlattices Microstruct.* **2021**, *151*, 106815, doi:10.1016/j.spmi.2021.106815.
29. Johs, B.D.; Hale, J.; Ianno, N.J.; Herzinger, C.M.; Tiwald, T.E.; Woollam, J.A. Recent developments in spectroscopic ellipsometry for in situ applications.; Duparre, A., Singh, B., Eds.; 2001; pp. 41–57.
30. Cherfi, D.E.; Guemmaz, M.; Bourahli, M.E.H.; Ouadfel, M.A.; Maabed, S. Effects of Nitrogen Flow Rate on the Structural, Morphological and Optical Properties of TaN Thin Films Grown by the DC Magnetron Sputtered Technique. *Acta Phys. Pol. A* **2019**, *136*, 849–854, doi:10.12693/APhysPolA.136.849.
31. Xu, H.; Hu, Z.-J.; Qu, X.-P.; Wan, H.; Yan, S.-S.; Li, M.; Chen, S.-M.; Zhao, Y.-H.; Zhang, J.; Baklanov, M.R. Effect of thickness scaling on the permeability and thermal stability of Ta(N) diffusion barrier. *Appl. Surf. Sci.* **2019**, *498*, 143887, doi:10.1016/j.apsusc.2019.143887.
32. Shamiryan, D.; Baklanov, M.R.; Maex, K. Diffusion barrier integrity evaluation by ellipsometric porosimetry. *J. Vac. Sci. Technol. B Microelectron. Nanom. Struct.* **2003**, *21*, 220, doi:10.1116/1.1539067.
33. Kondoh, E. *ELLIPSHEET, Mar. 1999; Final Rev Mar. 2011; http://www.ccn.yamanashi.ac.jp/~kondoh/ellips.html*;
34. Lee, K.; Lee, K. Optical Properties and X-ray Photoelectron Spectroscopy Study ofReactive-sputtered Ta-N Thin Films. *J. Korean Phys. Soc.* **2009**, *55*, 966–970, doi:10.3938/jkps.55.966.
35. Arshi, N.; Lu, J.; Joo, Y.K.; Yoon, J.H.; Koo, B.H. Effects of nitrogen composition on the resistivity of reactively sputtered TaN thin films. *Surf. Interface Anal.* **2015**, *47*, 154–160, doi:10.1002/sia.5691.
36. Cheviot, M.; Gouné, M.; Poulon-Quintin, A. Monitoring tantalum nitride thin film structure by reactive RF magnetron sputtering: Influence of processing parameters. *Surf. Coatings Technol.* **2015**, *284*, 192–197, doi:10.1016/j.surfcoat.2015.08.075.
37. Schauer, A.; Roschy, M. R.F. sputtered β-tantalum and b.c.c. tantalum films. *Thin Solid Films* **1972**, *12*, 313–317, doi:10.1016/0040-6090(72)90095-8.

38. Cuong, N.D.; Kim, D.-J.; Kang, B.-D.; Kim, C.S.; Yu, K.-M.; Yoon, S.-G. Characterization of Tantalum Nitride Thin Films Deposited on SiO[sub 2]/Si Substrates Using dc Magnetron Sputtering for Thin Film Resistors. *J. Electrochem. Soc.* **2006**, *153*, G164, doi:10.1149/1.2146861.
39. Arshi, N.; Lu, J.; Lee, C.G.; Koo, B.H.; Ahmed, F. Effects of Nitrogen Content on the Phase and Resistivity of TaN Thin Films Deposited by Electron Beam Evaporation. *JOM* **2014**, *66*, 1893–1899, doi:10.1007/s11837-014-1028-6.
40. Rossnagel, S.M. Characteristics of ultrathin Ta and TaN films. *J. Vac. Sci. Technol. B Microelectron. Nanom. Struct.* **2002**, *20*, 2328, doi:10.1116/1.1520556.
41. Lu, Y..; Weng, R..; Hwang, W..; Yang, Y.. Study of phase transition and electrical resistivity of tantalum nitride films prepared by DC magnetron sputtering with OES detection system. *Thin Solid Films* **2001**, *398–399*, 356–360, doi:10.1016/S0040-6090(01)01342-6.
42. Oku, T.; Kawakami, E.; Uekubo, M.; Takahiro, K.; Yamaguchi, S.; Murakami, M. Diffusion barrier property of TaN between Si and Cu. *Appl. Surf. Sci.* **1996**, *99*, 265–272, doi:10.1016/0169-4332(96)00464-3.
43. Willmott, D.J. Effect of nitrogen on the electrical and structural properties of triode-sputtered tantalum films. *J. Appl. Phys.* **1972**, *43*, 4865–4871, doi:10.1063/1.1661039.
44. Nie, H.B.; Xu, S.Y.; Wang, S.J.; You, L.P.; Yang, Z.; Ong, C.K.; Li, J.; Liew, T.Y.F. Structural and electrical properties of tantalum nitride thin films fabricated by using reactive radio-frequency magnetron sputtering. *Appl. Phys. A Mater. Sci. Process.* **2001**, *73*, 229–236, doi:10.1007/s003390000691.
45. Riekkinen, T.; Molarius, J.; Laurila, T.; Nurmela, A.; Suni, I.; Kivilahti, J.. Reactive sputter deposition and properties of TaxN thin films. *Microelectron. Eng.* **2002**, *64*, 289–297, doi:10.1016/S0167-9317(02)00801-8.
46. Sun, X.; Kolawa, E.; Chen, J.-S.; Reid, J.S.; Nicolet, M.-A. Properties of reactively sputter-deposited Ta◎N thin films. *Thin Solid Films* **1993**, *236*, 347–351, doi:10.1016/0040-6090(93)90694-K.
47. Stampfl, C.; Freeman, A.J. Stable and metastable structures of the multiphase tantalum nitride system. *Phys. Rev. B* **2005**, *71*, 024111, doi:10.1103/PhysRevB.71.024111.
48. Ishikawa, A.; Takata, T.; Matsumura, T.; Kondo, J.N.; Hara, M.; Kobayashi, H.; Domen, K. Oxysulfides Ln 2 Ti 2 S 2 O 5 as Stable Photocatalysts for Water Oxidation and Reduction under Visible-Light Irradiation. *J. Phys. Chem. B* **2004**, *108*, 2637–2642, doi:10.1021/jp036890x.
49. Fang, Z.; Aspinall, H.C.; Odedra, R.; Potter, R.J. Atomic layer deposition of TaN and Ta3N5 using pentakis(dimethylamino)tantalum and either ammonia or monomethylhydrazine. *J. Cryst. Growth* **2011**, *331*, 33–39, doi:10.1016/j.jcrysgro.2011.07.012.
50. Stampfl, C.; Freeman, A.J. Metallic to insulating nature of TaNx: Role of Ta and N vacancies. *Phys. Rev. B* **2003**, *67*, 064108, doi:10.1103/PhysRevB.67.064108.
51. Wang, C.; Hisatomi, T.; Minegishi, T.; Nakabayashi, M.; Shibata, N.; Katayama, M.; Domen, K. Thin film transfer for the fabrication of tantalum nitride photoelectrodes with controllable layered structures for water splitting. *Chem. Sci.* **2016**, *7*, 5821–5826, doi:10.1039/C6SC01763K.
52. Cherfi, D.E.; Guemmaz, M.; Bourahli, M.E.H.; Ouadfel, M.A.; Maabed, S. Effects of Nitrogen Flow Rate on the Structural, Morphological and Optical Properties of TaN Thin Films Grown by the DC Magnetron Sputtered Technique. *Acta Phys. Pol. A* **2019**, *136*, 849–854, doi:10.12693/APhysPolA.136.849.
53. Hashizume, T.; Saiki, A.; Terayama, K. Fabrication of Tantalum nitride thin film using the low vacuum magnetron sputtering system. *IOP Conf. Ser. Mater. Sci. Eng.* **2011**, *18*, 092032, doi:10.1088/1757-899X/18/9/092032.
54. Sung, Y.-M.; Kim, H.-J. Optimum substrate bias condition for TiN thin film deposition using an ECR sputter system. *Surf. Coatings Technol.* **2003**, *171*, 75–82, doi:10.1016/S0257-8972(03)00241-X.

55. Chang, C.-C.; Jeng, J..; Chen, J.. Microstructural and electrical characteristics of reactively sputtered Ta-N thin films. *Thin Solid Films* **2002**, *413*, 46–51, doi:10.1016/S0040-6090(02)00342-5.
56. Chuang, J.; Chen, M. Passivation of Cu by Sputter-Deposited Ta and Reactively Sputter-Deposited Ta-Nitride Layers. *J. Electrochem. Soc.* **1998**, *145*, 3170–3177, doi:10.1149/1.1838782.
57. Liu, X.; Ma, G.J.; Sun, G.; Duan, Y.P.; Liu, S.H. Effect of deposition and annealing temperature on mechanical properties of TaN film. *Appl. Surf. Sci.* **2011**, *258*, 1033–1037, doi:10.1016/j.apsusc.2011.08.116.
58. Sreenivasan, R.; Sugawara, T.; Saraswat, K.C.; McIntyre, P.C. High temperature phase transformation of tantalum nitride films deposited by plasma enhanced atomic layer deposition for gate electrode applications. *Appl. Phys. Lett.* **2007**, *90*, 102101, doi:10.1063/1.2643085.
59. Chun, W.-J.; Ishikawa, A.; Fujisawa, H.; Takata, T.; Kondo, J.N.; Hara, M.; Kawai, M.; Matsumoto, Y.; Domen, K. Conduction and Valence Band Positions of Ta 2 O 5 , TaON, and Ta 3 N 5 by UPS and Electrochemical Methods. *J. Phys. Chem. B* **2003**, *107*, 1798–1803, doi:10.1021/jp027593f.
60. Bertóti, I. Characterization of nitride coatings by XPS. *Surf. Coatings Technol.* **2002**, *151–152*, 194–203, doi:10.1016/S0257-8972(01)01619-X.
61. Nyholm, R.; Berndtsson, A.; Martensson, N. Core level binding energies for the elements Hf to Bi (Z=72-83). *J. Phys. C Solid State Phys.* **1980**, *13*, L1091–L1096, doi:10.1088/0022-3719/13/36/009.
62. Tian, X.; Gong, C.; Huang, Y.; Jiang, H.; Yang, S.; Fu, R.K.Y.; Chu, P.K. Ion trajectories in plasma ion implantation of slender cylindrical bores using a small inner end source. *Appl. Phys. Lett.* **2008**, *93*, 191501, doi:10.1063/1.2988192.
63. Tompkins, H.G.; Zhu, T.; Chen, E. Determining thickness of thin metal films with spectroscopic ellipsometry for applications in magnetic random-access memory. *J. Vac. Sci. Technol. A Vacuum, Surfaces, Film.* **1998**, *16*, 1297–1302, doi:10.1116/1.581277.